**Wei Luo***, **Jianguo Jiang**

J. Electrical Systems 10-3 (2014): 263-275

**Regular paper**

# Optimized Predictive Control of Three-Level Neutral Point Clamped Converter Based STATCOM Using Space-Vector Modulation

This paper presents the optimized predictive control of three-level neutral point clamped (NPC) converter based STATCOM intended for installation on renewable energy equipment, industrial and utility distribution systems. The optimized predictive control method computes the optimal vector using the converter's discrete-time model just once in every control cycle, while model predictive methods need 27 calculations. The main feature of the designed optimized predictive control scheme is to maintain the dc-bus voltage at the required level and to compensate the desired reactive power of systems. Meanwhile, the control technique operates with constant switching frequency, using space-vector modulation. Also, the paper solves time delay problem in real implementation by considering the delay compensation in the predictive model. As a result, the STATCOM operates with good performances in steady and transient states. Finally, both simulation and experimental results are shown the effectiveness of the STATCOM, and verified the validity of the proposed optimized predictive control method.

Keywords: Optimized Predictive Control; Three-Level NPC Converter; STATCOM; Delay Compensation; Space-Vector Modulation.

## 1. Introduction

Along with the optimized development of the power market, demands for power supply's quality and reliability become more and more strict. As an important reactive power compensation device in the flexible ac transmission system (FACTS), static synchronous compensator (STATCOM) has superior control performance and compensation effect, as well as ability to control power factor [1], [2]. Using a voltage source converter (VSC) as a variable source of reactive power is the most advanced solution to compensate reactive power, while the conventional two-level VSC have been widely used during the last decades [1]-[3]. For instance, a two-level multi-pulse topology is adopted in +100MVA STATCOM at the Tennessee Valley Authority (TVA) Sullivan substation, USA [4], [5].

Since the three-level NPC converter was invented in 1980 [6], lots of research has been worked on the three-level neutral point clamped (NPC) converter, along with their applications to industry and utility [7]-[9]. As a result, achieving the application of the STATCOM in the power system with a high voltage level is possible. Contrary to the two-level VSC, the three-level VSC is advantageous for STATCOM realization since it provides higher grid side voltage levels and improves compensation waveforms in terms of total harmonic distortion. So, this paper adopted the three-level NPC converter based STATCOM for the application. Meanwhile, The STATCOM operates with the space-vector modulation (SVM) method. As it brings lots of benefits compare to sinusoidal pulse width modulation (SPWM) techniques, such as lower demand of dc-bus voltage for a specified grid voltage and lower total harmonic distortion[9]-[11].

* Corresponding author: Wei Luo, Key Laboratory of Control of Power Transmission and Conversion, Ministry of Education (Department of Electrical Engineering, Shanghai Jiao Tong University), Shanghai 200030, China, E-mail: johnnyluo@sjtu.edu.cn

Recently, the significant development of microprocessors such as digital signal processors (DSPs) and field programmable gate arrays (FPGAs), makes is possible to implement new and more complex control techniques, for example, fuzzy logic, adaptive control, sliding mode control, and predictive control[12]-[14]. Among them, predictive control is becoming a more attractive control scheme for power converters due to its understandable concepts, optimized transient response and wide range of application [15].

The predictive control techniques applied to power electronics have been classified into two main categories: continuous control set and finite control set [15]-[18]. Ref. [19] gives an SVM based predictive current controller for inverters in distributed generation systems, and it proves that the continuous control set predictive control has an excellent steady state response as well as an extremely optimized dynamic response. In [20]-[23], finite control set predictive control is applied to three-level NPC VSC and two-level VSC, respectively. The main advantage of this method is that it does not require any kind of modulation technique, achieving a different approach to control the power converter. This paper proposes the continuous control set optimized predictive control method. A discrete model including delay compensation is used to predict the behaviour of the STATCOM for every two sampling period, and then the SVM modulator generates the switching states from the continuous output of the optimized predictive controller [24],[25].

In this dissertation, research is focusing on the optimized predictive control of three-level NPC converter based STATCOM using SVM technique, organizing as follows. The discrete-time model of STATCOM including the delay compensation is presented in section 2. Section 3 shows the optimized predictive control principle, and the major steps of proposed optimized predictive control algorithm are given in this section. Simulation studies of the proposed strategy are shown in section 4. Then, experimental results are presented to validate the theoretical studies in section 5. And finally, some conclusions are drawn in Section 6.

## 2. Notation

The notation used throughout the paper is stated below.

*Indexes:*

| | |
|---|---|
| $\boldsymbol{e}_s$ | three-phase grid voltage vector (V) |
| $e_{sd}$ $e_{sq}$ | three-phase grid voltage in *d-q* coordinate (V) |
| $\boldsymbol{u}_s$ | voltage vector generated by the STATCOM (V) |
| $u_{sd}$ $u_{sq}$ | voltage generated by the STATCOM in *d-q* coordinate (V) |
| $\boldsymbol{i}_c$ | compensation current vector (A) |
| $i_{cd}$ $i_{cq}$ | compensation current in *d-q* coordinate (A) |
| $\omega$ | angular frequency of grid voltage (rad/s) |
| $L_c$ | AC-link inductance (mH) |
| $v_{sd}$ $v_{sq}$ | defined voltage in *d-q* coordinate (V) |
| $T_s$ | sampling time (s) |
| $T_d$ | control delay time (s) |
| $f$ | grid frequency (Hz) |
| $C$ | DC-link capacitor (μF) |
| $u_{dc}$ | DC-link voltage (V) |
| $f_s$ | carrier frequency (Hz) |
| FACTS | flexible ac transmission system |

| | |
|---|---|
| STATCOM | static synchronous compensator |
| VSC | voltage source converter |
| NPC | neutral point clamped |
| SVM | space-vector modulation |
| SPWM | sinusoidal pulse width modulation |
| DSPs | digital signal processors |
| FPGAs | field programmable gate arrays |

## 3. Converter Model

### 3.1. Three-Level Converter Based STATCOM Model

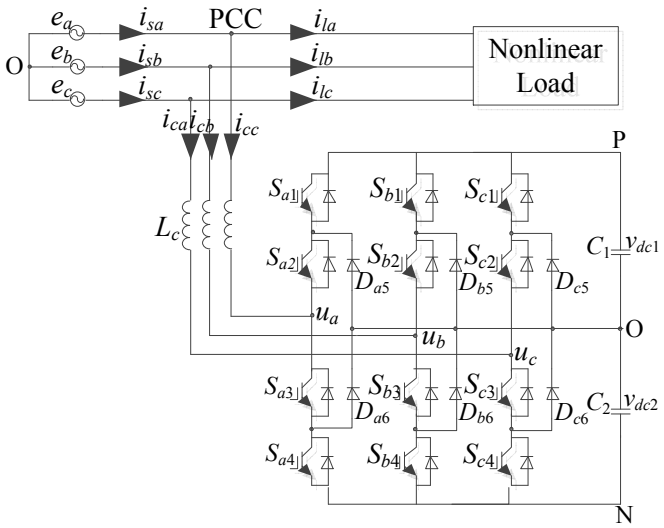


Fig.1. The topology of the three-level converter based STATCOM.

The topology of the three-level NPC converter based STATCOM is shown in Fig.1. It has twelve Insulated Gate Bipolar Transistors (IGBT's) and twelve freewheeling diodes, along with six clamp diodes arranged in a three-level NPC converter, connecting the three-phase gird voltage to the DC voltage. The reactive power caused by the nonlinear load can be eliminated by controlling the phase and amplitude of the STATCOM compensation voltage.

In a balanced three-phase system, neglecting the line resistance, the STATCOM compensation current dynamics can be expressed by the vector equation

$$L_c \frac{\mathrm{d}\mathbf{i}_c}{\mathrm{d}t} = \mathbf{e}_s - \mathbf{u}_s \tag{1}$$

where $\mathbf{i}_c$ is the compensation current vector, $\mathbf{e}_s$ is the three-phase grid voltage vector and $\mathbf{u}_s$ is the voltage vector generated by the STATCOM.

In the rotating *d-q* reference frame, the compensation currents equation can be described as

$$\begin{cases} \dfrac{di_{cd}}{dt} = \dfrac{1}{L_c}\left(e_{sd} - u_{sd} + \omega \bullet L_c \bullet i_{cq}\right) \\ \dfrac{di_{cq}}{dt} = \dfrac{1}{L_c}\left(e_{sq} - u_{sq} - \omega \bullet L_c \bullet i_{cd}\right) \end{cases} \tag{2}$$

In order to decouple the above differential equations, assuming that

$$\begin{cases} v_{sd} = u_{sd} - \omega \bullet L_c \bullet i_{cq} \\ v_{sq} = u_{sq} + \omega \bullet L_c \bullet i_{cd} \end{cases} \tag{3}$$

and replacing (3) in (2), the decoupled compensation currents equation is obtained

$$\begin{cases} \dfrac{di_{cd}}{dt} = \dfrac{1}{L_c}\left(e_{sd} - v_{sd}\right) \\ \dfrac{di_{cq}}{dt} = \dfrac{1}{L_c}\left(e_{sq} - v_{sq}\right) \end{cases} \tag{4}$$

### 3.2. Discrete-Time Model

A discrete-time model of the compensation current for a sampling time $T_s$ can be used to predict the future value of compensation current with the measured grid voltages and compensation currents at the $k$th sampling instant.

Approximating the derivative as the difference over one sampling instant

$$\frac{\mathrm{d}\mathbf{i}_c}{\mathrm{d}t} \approx \frac{\mathbf{i}_c(k+1) - \mathbf{i}_c(k)}{T_s} \tag{5}$$

and replacing it in(4), the future compensation current is obtained by the following expression

$$\begin{cases} i_{cd}(k+1) = i_{cd}(k) + \dfrac{T_s}{L_c}\left(e_{sd}(k) - v_{sd}(k)\right) \\ i_{cq}(k+1) = i_{cq}(k) + \dfrac{T_s}{L_c}\left(e_{sq}(k) - v_{sq}(k)\right) \end{cases} \tag{6}$$

where $e_{sd\text{-}q}$ and $i_{cd\text{-}q}$ are the grid voltages and compensation currents in rotating $d$-$q$ coordinates, respectively.

### 3.3. Delay Compensation

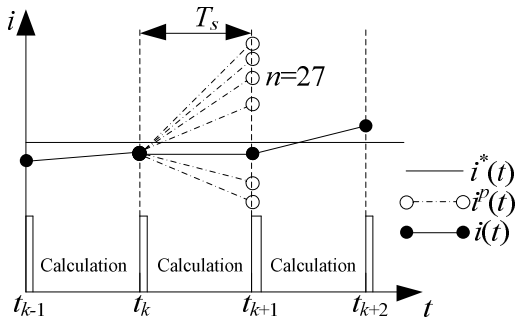


Fig.2. The principle of PCC (ideal case).

In a real-time implementation, a large number of calculations are needed, bringing in the time delay that can deteriorate the performance of the STATCOM. As shown in (6), the predictions of compensation currents in rotating $d$-$q$ coordinates are calculated using the measured grid voltages and compensation currents, assuming that the converter voltages are applied immediately in the ideal case. As shown in Fig.2, the switching state applied at $t_k$ is determined at $t_{k\text{-}1}$, and the voltages and currents are measured at $t_k$ , calculating the

predictive currents and the switching state which are applied at $t_{k+1}$ instantly. Therefore, when a one-sample horizon algorithm is considered, the time delay has a large impact on the prediction. This problem can be solved by implementing the delay compensation scheme.

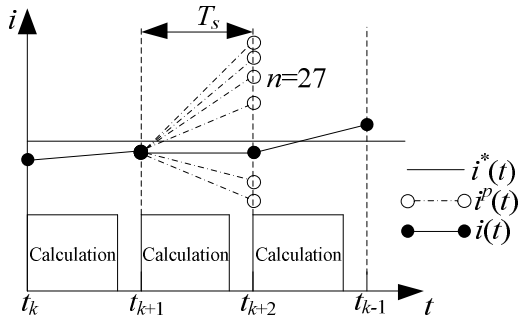


Fig.3. The principle of PCC (real case) with delay compensation.

The principle of optimized predictive control (real case) with delay compensation is shown in Fig.3. Note that the measured voltages and currents with the switching state at $t_k$ are used in (6) to estimate the current at $t_{k+1}$, then calculating the switching state at $t_{k+2}$. The predictions can be achieved by shifting (6) one step forward in time

$$\begin{cases} i_{cd}(k+2) = i_{cd}(k+1) + \dfrac{T_s}{L_c}\left(e_{sd}(k+1) - v_{sd}(k+1)\right) \\ i_{cq}(k+2) = i_{cq}(k+1) + \dfrac{T_s}{L_c}\left(e_{sq}(k+1) - v_{sq}(k+1)\right) \end{cases} \tag{7}$$

where $i_{cd\text{-}q}$ $(k+1)$ are the estimated compensation currents vector using the measured voltages and currents along with the converter voltages $v_{sd\text{-}q}$ $(k)$ applied in the previous sampling time.

## 4. Optimized Predictive Control Principle

### 4.1. Discrete-Time State-Space Equations of Control System

Assuming that the sampling interval is small enough: 1) the grid voltage vector maintains constant at its average value; 2) the STATCOM output voltage vector is constant; 3) the control delay time $T_d$ is defined as

$$T_d = (1-m)T_s, (0 \le m \le 1) \tag{8}$$

Then the discrete-time model of the three-phase three-level NPC converter based STATCOM in *d-q* coordinate with the control delay can be derived as

$$\mathbf{E}(n+1) = \mathbf{\Phi} \bullet \mathbf{E}(n) + \mathbf{\Psi}_0 \bullet \mathbf{X}_1(n) + \mathbf{\Psi}_1 \bullet \mathbf{X}_1(n-1) - \mathbf{\Psi} \bullet \mathbf{X}_2(n) \tag{9}$$

where the matrices are given by

$$\begin{aligned} &\mathbf{\Phi} = e^{\mathbf{A}T_s}; \mathbf{\Psi}_0 = \int_0^{mT_s} e^{\mathbf{A}t}\mathbf{B}dt; \\ &\mathbf{\Psi}_1 = \int_{mT_s}^{T_s} e^{At}\mathbf{B}dt; \mathbf{\Psi} = \int_0^{T_s} e^{At}\mathbf{B}dt; \end{aligned} \tag{10}$$

where

$$\mathbf{A}=\begin{bmatrix}0 & \omega\\ -\omega & 0\end{bmatrix};\mathbf{B}=\begin{bmatrix}1/L_c & 0\\ 0 & 1/L_c\end{bmatrix}; \tag{11}$$

and replacing (11) in (10), we can obtained

$$\begin{aligned}
\mathbf{\Phi}&=\begin{bmatrix}\cos(\omega T_s) & \sin(\omega T_s)\\ -\sin(\omega T_s) & \cos(\omega T_s)\end{bmatrix};\\
\mathbf{\Psi}_0&=\frac{1}{\omega L_c}\begin{bmatrix}\sin(m\omega T_s) & 1-\cos(m\omega T_s)\\ \cos(m\omega T_s)-1 & \sin(m\omega T_s)\end{bmatrix};\\
\mathbf{\Psi}_1&=\frac{1}{\omega L_c}\begin{bmatrix}\sin(\omega T_s)-\sin(m\omega T_s) & -\cos(\omega T_s)+\cos(m\omega T_s)\\ \cos(\omega T_s)-\cos(m\omega T_s) & \sin(\omega T_s)-\sin(m\omega T_s)\end{bmatrix};\\
\mathbf{\Psi}&=\frac{1}{\omega L_c}\begin{bmatrix}\sin(\omega T_s) & 1-\cos(\omega T_s)\\ \cos(\omega T_s)-1 & \sin(\omega T_s)\end{bmatrix};
\end{aligned} \tag{12}$$

The optimized predictive controller is designed for the current references to generate the desired converter output voltage references. From (7) and (9), the discrete-time state-space equations of optimized predictive control system using SVM can be derived as

$$\begin{bmatrix}\mathbf{E}(n+1)\\ \mathbf{E}^p(n+1)\\ \mathbf{E}^*(n)\\ \mathbf{X}_2(n)\end{bmatrix}=\begin{bmatrix}\mathbf{G} & \mathbf{H}_1\\ \mathbf{0} & \mathbf{0}\end{bmatrix}\begin{bmatrix}\mathbf{E}(n)\\ \mathbf{E}^p(n)\\ \mathbf{E}^*(n-1)\\ \mathbf{X}_2(n-1)\end{bmatrix}+\begin{bmatrix}\mathbf{H}_0\\ \mathbf{I}\end{bmatrix}\begin{bmatrix}\mathbf{E}^*(n)\\ \mathbf{X}_2(n)\end{bmatrix} \tag{13}$$

where "**0**" represents zero matrix, "**I**" represents unity matrix, matrices **G**, $\mathbf{H}_1$, and $\mathbf{H}_0$ are gi ven in (14)-(16), respectively.

$$\mathbf{G}=\begin{bmatrix}g_{11} & g_{12} & g_{13} & g_{14}\\ g_{21} & g_{22} & g_{23} & g_{24}\\ 1 & 0 & 0 & 0\\ 0 & 1 & 0 & 0\end{bmatrix} \tag{14}$$

where

$$\begin{aligned}
g_{11}&=g_{22}=\cos(\omega T_s)+\frac{1}{L_c}\left(-\frac{\sin(m\omega T_s)}{\omega T_s}+\frac{1-\cos(m\omega T_s)}{2}\right)\\
g_{12}&=-g_{21}=\sin(\omega T_s)-\frac{1}{L_c}\left(\frac{\sin(m\omega T_s)}{2}+\frac{1-\cos(m\omega T_s)}{\omega T_s}\right)\\
g_{13}&=g_{24}=\frac{1}{L_c}\left(\frac{-\sin(\omega T_s)+\sin(m\omega T_s)}{\omega T_s}+\frac{-\cos(\omega T_s)+\cos(m\omega T_s)}{2}\right)\\
g_{14}&=-g_{23}=\frac{1}{L_c}\left(\frac{-\sin(\omega T_s)+\sin(m\omega T_s)}{2}+\frac{\cos(\omega T_s)-\cos(m\omega T_s)}{\omega T_s}\right)
\end{aligned}$$

$$\mathbf{H}_0=\begin{bmatrix}h_{011} & h_{012} & h_{013} & h_{014}\\ h_{021} & h_{022} & h_{023} & h_{024}\\ 0 & 0 & 0 & 0\\ 0 & 0 & 0 & 0\end{bmatrix} \tag{15}$$

where

$$h_{011}=h_{022}=\frac{1}{L_c}\left(\frac{\sin\left(m\omega T_s\right)}{\omega T_s}+\frac{1-\cos\left(m\omega T_s\right)}{2}\right)$$

$$h_{012}=-h_{021}=\frac{1}{L_c}\left(-\frac{\sin\left(m\omega T_s\right)}{2}+\frac{1-\cos\left(m\omega T_s\right)}{\omega T_s}\right)$$

$$h_{013}=h_{024}=\frac{-\sin\left(\omega T_s\right)+\sin\left(m\omega T_s\right)}{\omega L_c}$$

$$h_{014}=-h_{023}=\frac{\cos\left(\omega T_s\right)-\cos\left(m\omega T_s\right)}{\omega L_c}$$

$$\mathbf{H}_1=\begin{bmatrix} h_{111} & h_{112} & h_{113} & h_{114} \\ h_{121} & h_{122} & h_{123} & h_{124} \\ 0 & 0 & 0 & 0 \\ 0 & 0 & 0 & 0 \end{bmatrix} \tag{16}$$

where

$$h_{111}=h_{122}=\frac{1}{L_c}\left(\frac{\sin\left(\omega T_s\right)-\sin\left(m\omega T_s\right)}{\omega T_s}+\frac{-\cos\left(\omega T_s\right)+\cos\left(m\omega T_s\right)}{2}\right)$$

$$h_{112}=-h_{121}=-\frac{1}{L_c}\left(\frac{\sin\left(\omega T_s\right)-\sin\left(m\omega T_s\right)}{2}+\frac{\cos\left(\omega T_s\right)-\cos\left(m\omega T_s\right)}{\omega T_s}\right)$$

$$h_{113}=h_{124}=\frac{\sin\left(\omega T_s\right)-\sin\left(m\omega T_s\right)}{\omega L_c}$$

$$h_{114}=-h_{123}=\frac{-\cos\left(\omega T_s\right)+\cos\left(m\omega T_s\right)}{\omega L_c}$$

## 4.2. Optimized Predictive Control System

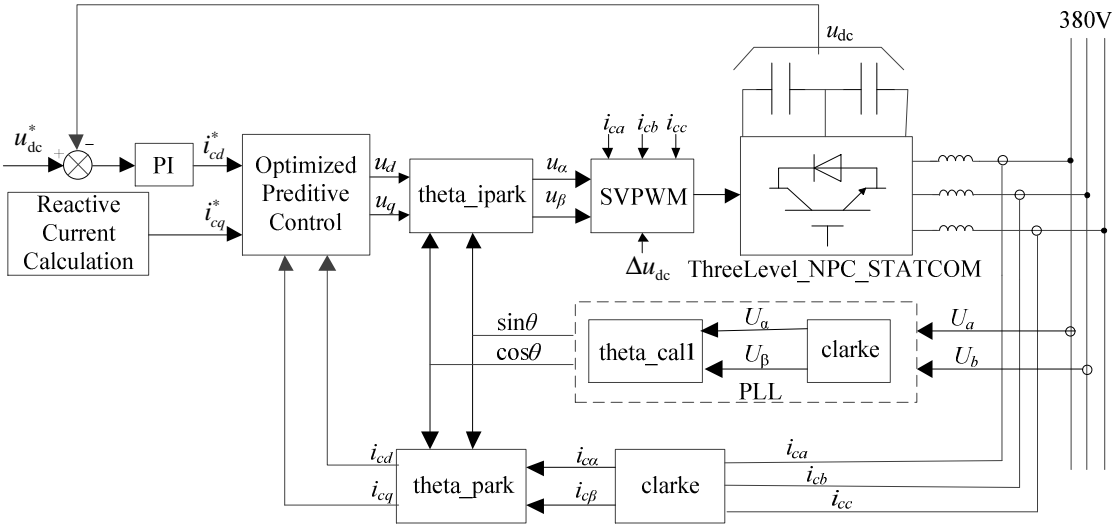


Fig.4. The optimized predictive control block diagram.

Fig.4 shows the configuration of the proposed optimized predictive control. In this scheme, command of compensation current vector component is determined by the reactive current

calculation part, and command of compensation current vector component is delivered from the proportional-integral dc-bus voltage controller. And then, together with the measured grid voltage vectors $e_{d\text{-}q}$ and compensation current vectors $i_{cd\text{-}q}$, they are used as input variables of the optimized predictive control algorithm block. In order to make sure that the compensation current vector at the next two sampling instant equal to the command reference value, obtaining the following equations:

$$\begin{cases} i_{cd}(k+2) = i_{cd}^{*}(k+2) \\ i_{cq}(k+2) = i_{cq}^{*}(k+2) \end{cases} \tag{17}$$

Assuming that the tracking error of dc-bus voltage is constant over two continuous sampling periods, the desired predicted value can be estimated using a linear extrapolation by the following expression:

$$i_{cd}^{*}(k+2) = 2i_{cd}^{*}(k+1) - i_{cd}^{*}(k) \tag{18}$$

On the other side, command of compensation current vector component is determined by the reactive current calculation part, assuming it is constant when the sampling interval is small enough:

$$i_{cq}^{*}(k+2) = i_{cq}^{*}(k+1) \tag{19}$$

Replacing (8), (9) and (10) in (7), the optimized predictive control formulas are obtained by the following expression:

$$\begin{cases} v_d(k) = e_{sd}(k) - \dfrac{L_c}{T_s}\left(2i_{cd}^{*}(k) - i_{cd}^{*}(k-1) - i_{cd}(k)\right) \\ v_q(k) = e_{sq}(k) - \dfrac{L_c}{T_s}\left(i_{cq}^{*}(k) - i_{cq}(k)\right) \end{cases} \tag{20}$$

Take (3) into the above formulas, we can acquire the desired converter voltage vectors:

$$\begin{cases} u_d(k) = e_{sd}(k) - \dfrac{L_c}{T_s}\left(2i_{cd}^{*}(k) - i_{cd}^{*}(k-1) - i_{cd}(k)\right) + \omega \bullet L_c \bullet i_{cq}(k) \\ u_q(k) = e_{sq}(k) - \dfrac{L_c}{T_s}\left(i_{cq}^{*}(k) - i_{cq}(k)\right) - \omega \bullet L_c \bullet i_{cd}(k) \end{cases} \tag{21}$$

Then the converter voltage vectors are transformed from rotating *d-q* coordinates to static $\alpha$-$\beta$ coordinates, later the reverse park transformation outputs are passed through SVM modulator, which provides the switch states for IGBT's.

The optimized predictive control algorithm in the paper contains five major steps:

(1) Measure the grid voltages, grid currents, compensation currents, dc-bus voltages and compute the reactive currents.

(2) Predict the compensation currents for the next two sampling periods.

(3) Evaluate the desired converter voltage vectors.

(4) Obtain the switching states using the SVM modulator.

(5) Apply the switching states for IGBT's.

## 5. Simulation Results

Optimized predictive control algorithms proposed in this paper have been simulated using software Matlab/Simulink. The main electrical parameters of the power circuit used

in simulation and implementation platforms are shown in Table1.The following simulation results are based on sinusoidal three-phase grid voltages.

**Table 1.** Electrical Parameters of the Power Circuit

| Parameters | Values |
|---|---|
| Line to line ac rms voltage, $e_{ab}$ | 380V |
| Grid frequency, $f$ | 50Hz |
| AC-link inductance, $L_c$ | 0.6mH |
| DC-link capacitor, $C$ | 1490μF |
| DC-link voltage, $u_{dc}$ | 570V |
| Carrier frequency, $f_s$ | 5kHz |

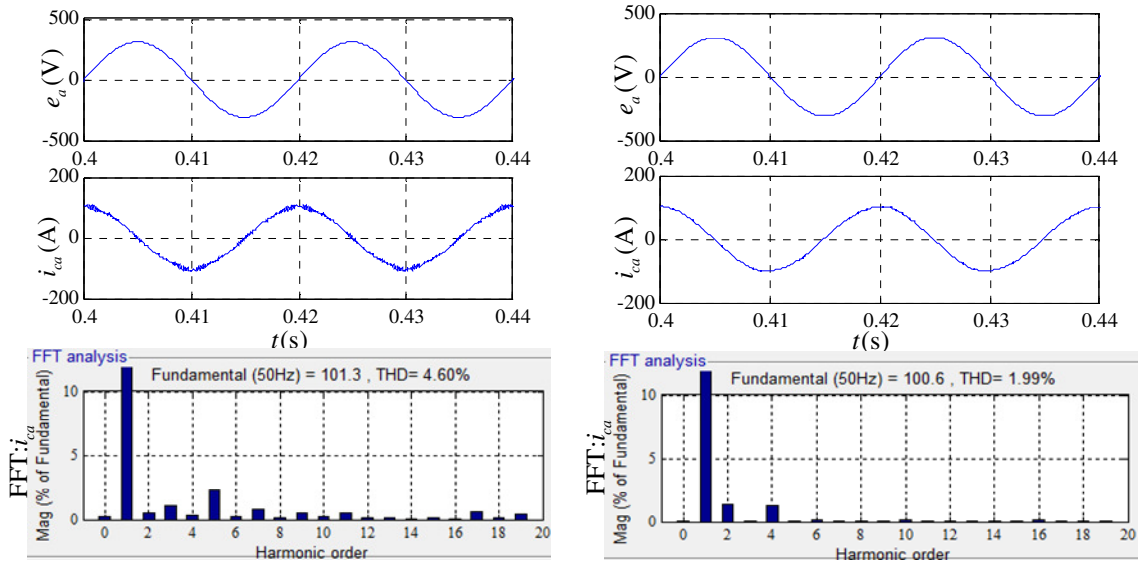


(a) (b)

Fig.5. Simulation results in steady state operation. (a) Without delay compensation. (b) With delay compensation.

Fig. 5 shows the simulation results of the STATCOM under steady state operation. Fig.5 (a) shows the grid voltage, the converter voltage, the compensation current and its FFT result when the predictive model does not include the delay compensation. When the delay compensation is considered in the predictive model, the total harmonic distortion (THD) of the compensation current can be considerably reduced, as shown in Fig. 5(b).

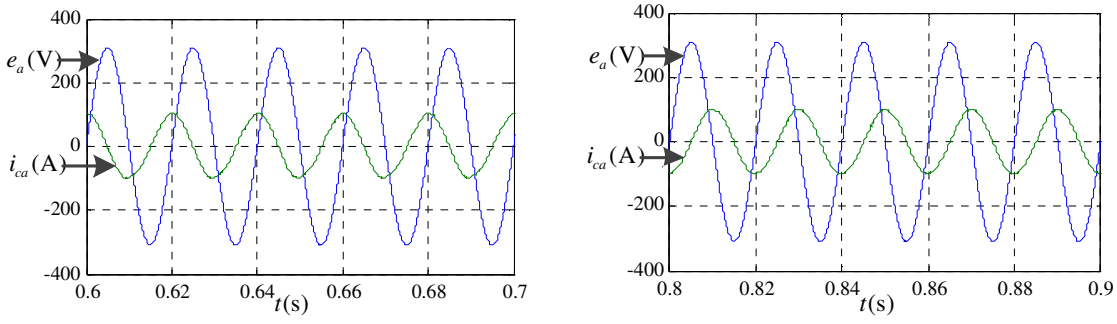


(a) (b)

Fig.6. Simulation results in steady state operation. (a) Under capacitive operation. (b) Under inductive operation.

The performance of the STATCOM under capacitive and inductive operation is shown in Fig.6. The compensation current, as shown in Fig.6 (a), is nearly sinusoidal and leading the

grid phase voltage by 90 degrees to compensate (offer) the needed capacitive power. On the other hand, Fig.6 (b) shows the compensation current is nearly sinusoidal and lagging the gird phase voltage by 90 degrees to compensate (offer) the needed inductive power. It is clear that both capacitive and inductive operation of three-level converter based STATCOM have good performance.

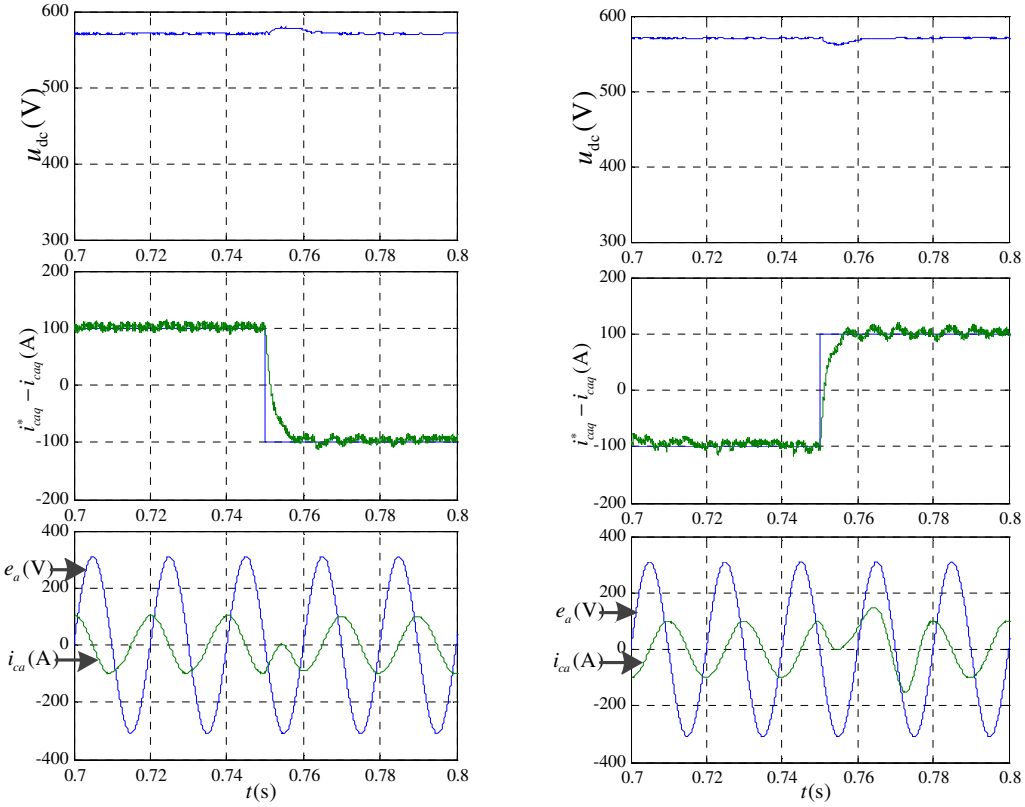


Fig.7. Simulation results in transient state operation. (a) Step in the reactive current from 100A to -100A. (b) Step in the reactive current from -100A to 100A.

Fig.7 shows the simulation waveforms in the transient state when a step changes from 100A to -100A and -100A to 100A of the reactive current reference. Note that when the reactive current reference equals to 100A means capacitive operation, while equals to -100A means inductive operation. It can be seen that the step response of reactive current is much optimized; the response time is less than 10ms. Also, the dc-bus voltage is very close to its reference value, operating with the satisfactory performance even in the transient state.

## 6. Experimental Results

In this section, the optimized predictive control algorithms have been carried out on a 200 kVA three-level converter based STATCOM. The specifications of the experimental system are the same as those used previously in Table1.The 200 kVA STATCOM experimental bench is consisting of a three-phase IGBTs(FF650R17IE4, INFINEON) and dual-channel drivers with fiber-optics(2SP0320V2A0, CONCEPT). As there are three line to line grid voltages($e_{ab}$, $e_{bc}$, $e_{ca}$), three phase grid currents($i_{sa}$, $i_{sb}$, $i_{sc}$), three phase compensation currents($i_{ca}$, $i_{cb}$, $i_{cc}$) and two dc-bus voltages($v_{dc1}$, $v_{dc2}$) to be measured, five voltage transducers (AV 100-1000, LEM) and six current transducers (LT508-S6, LEM) are used, respectively.

The control algorithms are implemented on a DSP (TMS320F28335, TEXAS INSTRUMENTS) and a FPGA (ProASIC3A3P250-FPGA). The control algorithms are divided into two parts, clarke transformation, park transformation, optimized predictive control, voltage vectors' selection and SVM has been executed in DSP, while the FPGA completes AD samplings and generates the firing pulses for IGBT's.

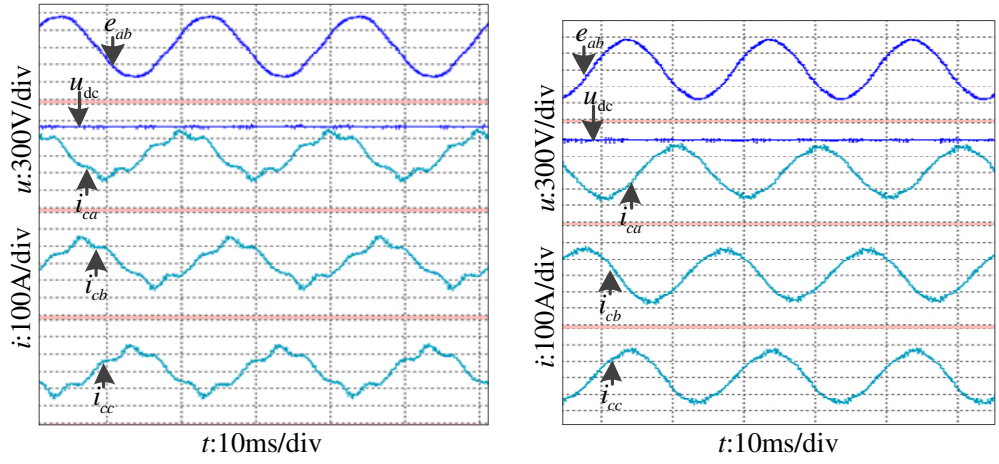


Fig.8. Experimental results in steady state operation. (a) Without delay compensation. (b) With delay compensation.

Fig. 8 shows the experimental results of the STATCOM under steady state operation. Fig.8 (a) shows the grid voltage, dc-bus voltage, the compensation current when the predictive model does not include the delay compensation. It is possible to observe that the total harmonic distortion (THD) of the compensation current can be considerably reduced when the delay compensation is considered in the predictive model, as shown in Fig. 8(b) Moreover, it can be seen that the dc-bus voltage is close to its reference value, operating with the good performance in the steady state.

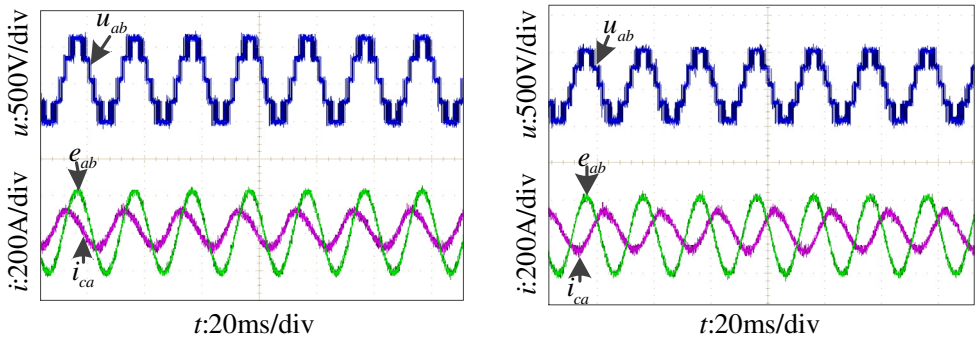


Fig.9. Experimental results in steady state operation. (a) Under capacitive operation. (b) Under inductive operation.

The performance of the STATCOM under capacitive and inductive operation is shown in Fig.9, including the gird line voltage, compensation current, and converter line voltage in steady state operation. Fig.9 (a) shows that the compensation current is nearly sinusoidal and leading the gird line voltage by 60 degrees to compensate the needed capacitive power. On the other hand, Fig.9 (b) shows the compensation current is nearly sinusoidal and lagging the grid line voltage by 120 degrees to compensate the needed inductive power. It can be

observed that both capacitive and inductive operation of three-level converter based STATCOM have good performance in experimental operation.

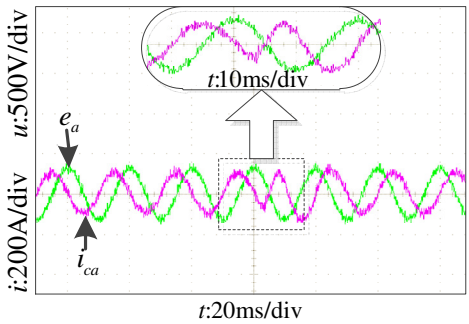


Fig.10. Experimental results in transient state operation. Step in the reactive current from 150A to -150A.

Fig.10 shows the experimental waveform in the transient state when a step changes from 150A to -150A of the reactive current reference. Also, when the reactive current reference equals to 150A means capacitive operation, while equals to -150A means inductive operation. It can be seen that the step response of reactive current is very optimized, the response time is less than 10ms.

## 7. Conclusion

This paper presents the optimized predictive control of three-level NPC converter based STATCOM, reducing the calculated amount of predictive control largely, especially for the multilevel converter. Meanwhile, the control technique operates with constant switching frequency, using space-vector modulation. Simulation results have proven the excellent performance of proposed optimized predictive control method, both in steady and transient states. Some implementation issues have been studied, such as compensation of the control delay, thus improving the performance of the optimized predictive control strategy by considering the delay compensation in the predictive model. Experimental results have been verified the effective of the proposed algorithm.

## Acknowledgment

This work was supported by the National High Technology Research and Development Programme of China (863 Programme) under Grant No.2011AA050403.

## References

[1] N.G.Hingorani, L.Gyugyi, “Understanding FACTS: concepts and technology of flexible AC transmission systems,” Wiley-IEEE Press, 1999, Chap1.

[2] J.Arrillaga, Y.H.Liu, and N.R.Watson, “Flexible Power Transmission: The HVDC Options,” Wiley-IEEE Press, 2007, Chap1.

[3] D.Soto, and T.C.Green, “A Comparison of High-Power Converter Topologies for the Implementation of FACTS Controllers,” IEEE Transactions on Industrial Electronics, vol.49, no.5, Oct.2002.

[4] C.Schauder, M.Gernhardt, E.Stacey, T.Lemak, L.Gyugyi, A.Edris, and T.W.Cease, “Development of a +100 MVAR Static Condenser for Voltage Control of Transmission Systems,” IEEE Transactions on Power Delivery, vol.10, no. 3, pp.1486-1493, Jul.1995.

[5] C.Schauder, M.Gernhardt, E.Stacey, T.Lemak, L.Gyugyi, T.W.Cease, and A.Edris, “Operation of +l00 MVAR

TVA Statcon," IEEE Transactions on Power Delivery, vol. 12, no. 4, pp1805-1811, Oct.1997.

[6] A.Nabae, I.Takahashi, and H.Akagi, "A new neutral- point-clamped PWM inverter," IEEE Transactions on Industry Applications, vol.IA-17, no.5, pp.518-523, Sep./Oct.1981.

[7] A.Lewicki, Z.Krzeminski, and H.Abu-Rub, "Space- Vector Pulsewidth Modulation for Three-Level NPC Converter with the Neutral Point Voltage Control," IEEE Transactions on Industrial Electronics, vol.58, no.11, pp5076-5086, Nov.2011.

[8] G.Abad, M.Á.Rodríguez, and J.Poza, "Three-Level NPC Converter-Based Predictive Direct Power Control of the Doubly Fed Induction Machine at Low Constant Switching Frequency," IEEE Transactions on Industrial Electronics, vol.55, no.12, pp.4417-4429, Dec.2008.

[9] R.Portillo, S.Vazquez, J.I.Leon, M.M.Prats, and L.G.Franquelo, "Model Based Adaptive Direct Power Control for Three-Level NPC Converters," IEEE Transactions on Industrial Informatics, vol.9, no.2, pp.1148-1157, May.2013.

[10] B.Singh, R.Saha, A.Chandra, K.Al-Haddad,"Static synchronous compensators (STATCOM)a review," IET Power Electronics, vol.2, iss.4, pp.297-324, 2009.

[11] M.Saeedifard, H.Nikkhajoei, and R.Iravani, "A Space Vector Modulated STATCOM Based on a Three-Level Neutral Point Clamped Converter," IEEE Transactions on Power Delivery, vol.22, no.2, pp.1029-1039, Apr.2007.

[12] J.Álvarez, Ó.López, F.D.Freijedo, and J.Doval-Gandoy, "Digital Parameterizable VHDL Module for Multilevel Multiphase Space Vector PWM," IEEE Transactions on Industrial Applications, vol.58, no.9, pp.3946-3957, Sep. 2011.

[13] M.Hamouda, H.F.Blanchette, K.Al-Haddad, and F.Fnaiech, "An Efficient DSP-FPGA-Based Real-Time Implementation Method of SVM Algorithms for an Indirect Matrix Converter," IEEE Transactions on Industrial Applications, vol.58, no.11, pp5024-5031, Nov.2011.

[14] E.Monmasson, L.Idkhajine, and M.W.Naouar, "FPGA- based controllers," IEEE Transactions on Industrial Magazine, vol.5, no.1, pp.14–26, Mar.2011.

[15] P.Cortés, M.P.Kazmierkowski, R.M.Kennel, D.E.Quevedo, and J.Rodríguez, "Predictive Control in Power Electronics and Drives," IEEE Transactions on Industry Electronics, vol.55, no.12, pp.4312-4324, Dec.2008.

[16] J.Rodríguez, M.P.Kazmierkowski, J.R.Espinoza, P.Zanchetta, H.Abu-Rub, H.A.Young, and C.A.Rojas, "State of the Art of Finite Control Set Model Predictive Control in Power Electronics," IEEE Transactions on Industry Informatics, vol.9, no.2, pp.1003-1016, May.2013.

[17] S.Kouro, P.Cortés, R.Vargas, U.Ammann, and J.Rodríguez, "Model predictive control-A simple and powerful method to control power converters," IEEE Transactions on Industry Electronics, vol.56, no.6, pp.1826-1838, Jun.2009.

[18] Shiroei, M , Ranjbar, AM, and Amraee, T, "A functional model predictive control approach for power system load frequency control considering generation rate constraint," International Transactions on Electrical Energy Systems, vol.23, no.2, pp.214-229, Mar.2013.

[19] Qingrong Zeng, and Liuchen Chang, "An Advanced SVPWM-Based Predictive Current Controller for Three-Phase Inverters in Distributed Generation Systems," IEEE Transactions on Industry Electronics, vol.55, no.3, pp.1235-1246, Mar.2008.

[20] R.Vargas, P.Cortés, U.Ammann, J.Rodríguez, and J.Pontt, "Predictive control of a three-phase neutral-point-clamped inverter," IEEE Transactions on Industry Electronics, vol.54, no.5, pp.2697–2705, Oct.2007.

[21] P.Cortés, J.Rodríguez, D.E.Quevedo, and C.Silva, "Predictive current control strategy with imposed load current spectrum," IEEE Transactions on Power Electronics, vol.23, no.2, pp.612-618, Mar.2008.

[22] Y.A.I.Mohamed, and E.F.El-Saadany, "Robust High Bandwidth Discrete-Time Predictive Current Control with Predictive Internal Model—A Unified Approach for Voltage-Source PWM Converters," IEEE Transactions on Power Electronics, vol.23, no.1, Jan.2008.

[23] D.E.Quevedo, R.P.Aguilera, M.A.Pérez, P.Cortés, and R.Lizana, "Model Predictive Control of an AFE Rectifier with Dynamic References," IEEE Transactions on Power Electronics, vol.27, no.7, Jul. 2012.

[24] A.Bouafia, J.Gaubert, F.Krima, "Design and implementation of predictive current control of three-phase PWM rectifier using space-vector modulation (SVM)," Energy Conversion and Management, vol.51, pp.2473-2481, 2010.

[25] P.Cortés, J.Rodríguez, C.Silva, and A.Flores, "Delay Compensation in Model Predictive Current Control of a Three-Phase Inverter," IEEE Transactions on Industry Electronics, vol.59, no.2, pp.1323-1325, Feb.2012.